J|A|C|S ARTICLES

Published on Web 10/16/2009

Ferrocenylhydridoborates: Synthesis, Structural Characterization, and Application to the Preparation of Ferrocenylborane Polymers

Matthias Scheibitz,[†] Haiyan Li,[‡] Jan Schnorr,[†] Alejandro Sánchez Perucha,[†] Michael Bolte,[†] Hans-Wolfram Lerner,[†] Frieder Jäkle,*[,‡] and Matthias Wagner*[,†]

Institut für Anorganische und Analytische Chemie, Johann Wolfgang Goethe-Universität Frankfurt, Max-von-Laue-Strasse 7, D-60438 Frankfurt am Main, Germany, and Department of Chemistry, Rutgers University Newark, 73 Warren Street, Newark, New Jersey 07102

Received August 4, 2009; E-mail: matthias.wagner@chemie.uni-frankfurt.de; fjaekle@rutgers.edu

Abstract: Mono- and ditopic lithium ferrocenylhydridoborates Li[FcBH$_3$] (**2**) and Li$_2$[H$_3$B-fc-BH$_3$] (**4**) have been synthesized from FcB(OMe)$_2$/(MeO)$_2$B-fc-B(OMe)$_2$ and Li[AlH$_4$] (Fc = ferrocenyl; fc = 1,1′-ferrocenylene). X-ray quality crystals were grown from OEt$_2$. Depending on the amount of Li$^+$-coordinated solvent molecules, dimeric (**2(OEt$_2$)$_2$**) or tetrameric (**2(OEt$_2$)**) aggregates are observed in the solid state. The ditopic derivative **4** crystallizes as two different macrocyclic dimers (**4(OEt$_2$)$_5$** and **4(OEt$_2$)$_6$**) in the unit cell. Each of the four aggregates is held together mainly by RBH$_3$-η^2-Li bonds. Addition of Me$_3$SiCl to **2** or **4** generates the corresponding boranes FcBH$_2$ (**5**) and H$_2$B-fc-BH$_2$ (**6**), which can be trapped by adduct formation with NMe$_2$Et or SMe$_2$. In contrast, when OEt$_2$ is present as the sole Lewis basic donor, no stable ether adducts are obtained, but condensation takes place leading to Fc$_2$BH (**10**) and the novel borane polymer [-fcB(H)-]$_n$ (**9**), respectively. In situ generation of FcBH$_2$ (**5**) in the presence of cyclohexene gives Fc$_2$BCy and BCy$_3$ but no FcBCy$_2$, thereby indicating that **5** undergoes condensation to **10** more quickly than hydroboration of an internal olefin can occur (Cy = cyclohexyl). Fc$_2$BH (**10**) was further studied as a model system for the optimization of modification reactions of polymer [-fcB(H)-]$_n$ (**9**). Hydroboration of PhCCH or *t*BuCCH with **10** proceeds smoothly and quantitatively to give the corresponding vinylboranes Fc$_2$B(CH=CHR) (**11^{Ph}**, R = Ph; **11^{tBu}**, R = *t*Bu), which were fully characterized. In a similar manner, the polymeric borane **9** was successfully transformed into ferrocenylborane polymers [-fcB(CH=CHR)-]$_n$ (**12^{Ph}**, R = Ph; **12^{tBu}**, R = *t*Bu) that contain vinyl groups attached to boron. The structures of polymers **12** were confirmed by NMR and IR spectroscopy and mass spectrometry. The MALDI-TOF spectra of **12^{Ph}** and **12^{tBu}** showed patterns of equidistant peaks with peak separations that are consistent with the masses of the expected repeating units of each of the polymers. The absorption maxima in the UV−vis spectra of polymers **12** are significantly red-shifted in comparison to the dimeric model systems **11**.

Introduction

Tetrahydridoborate, diborane, and borane-Lewis base adducts are abundant reducing agents in preparative chemistry.[1] The [BH$_4$]$^-$ ion has also been employed as ligand for a wide range of (transition) metal ions.[2,3] In the latter context, the tendency of [BH$_4$]$^-$ to form unusual covalent complexes that are volatile and/or soluble in unpolar solvents makes metal tetrahydroborates valuable precursors for the deposition of metal boride thin films.[4−6] Moreover, given that [BH$_4$]$^-$ ions have a propensity to adopt bridging positions between metal ions (cf. the polymeric structure of Be[BH$_4$]$_2$[7]), a use as building blocks for coordination polymers and low-dimensional solids can be envisaged.

However, it soon became apparent that replacement of hydrogen atoms in [BH$_4$]$^-$ or B$_2$H$_6$ by organic substituents greatly expands the range of applications, because the organic moiety in mono- and diorganylhydridoborates/boranes serves as an important set-screw for tuning their chemical properties. For example, compared to diborane, compounds such as thexylborane or 9-borabicyclo[3.3.1]nonane show a greatly enhanced regioselectivity in the hydroboration of olefins. Chiral derivatives like diisopinocampheylborane proved to be efficient reagents in asymmetric synthesis.[8] Also in the case of metal hydridoborate complexes, the presence of organyl groups should result in a modulation of the M···HB interaction(s) with impact on structural[9] and reactivity patterns.[10−15]

[†] Johann Wolfgang Goethe-Universität Frankfurt.
[‡] Rutgers University Newark.

(1) Pelter, A.; Smith, K.; Brown, H. C. *Borane Reagents*; Academic Press: London, 1988.
(2) Marks, T. J.; Kolb, J. R. *Chem. Rev.* **1977**, *77*, 263–293.
(3) Ephritikhine, M. *Chem. Rev.* **1997**, *97*, 2193–2242.
(4) Jensen, J. A.; Gozum, J. E.; Pollina, D. M.; Girolami, G. S. *J. Am. Chem. Soc.* **1988**, *110*, 1643–1644.
(5) White III, J. P.; Deng, H.; Shore, S. G. *Inorg. Chem.* **1991**, *30*, 2337–2342.
(6) Kumar, N.; Yang, Y.; Noh, W.; Girolami, G. S.; Abelson, J. R. *Chem. Mater.* **2007**, *19*, 3802–3807.
(7) Marynick, D. S.; Lipscomb, W. N. *Inorg. Chem.* **1972**, *11*, 820–823.
(8) Ramachandran, P. V.; Brown, H. C. *Organoboranes for Syntheses*; ACS Symposium Series 783; American Chemical Society: Washington, DC, 2001.
(9) Knizek, J.; Nöth, H. *J. Organomet. Chem.* **2000**, *614−615*, 168–187.

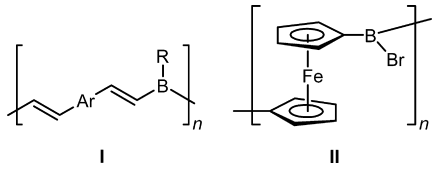

Figure 1. π-Conjugated polymers synthesized by hydroboration polymerization (**I**) and condensation polymerization (**II**).

In view of this rich chemistry, our groups became interested in the development of new classes of organylhydridoborates and organylboranes with a special focus on the following targets: (1) derivatives $[OM\text{-}BH_3]^-$ and $OM\text{-}BH_2(Do)$ with organometallic substituents OM (Do = Lewis basic donor) and (2) ditopic species $[H_3B\text{-}OM'\text{-}BH_3]^{2-}$ and $(Do)H_2B\text{-}OM'\text{-}BH_2(Do)$, in which two hydridoborate/borane functionalities are connected by an organometallic linker OM′.

The aimed-for hydridoborates $[OM\text{-}BH_3]^-$ and $[H_3B\text{-}OM'\text{-}BH_3]^{2-}$ not only are expected to serve as ideal starting materials for the synthesis of the corresponding boranes but also could function as interesting ligand molecules, because coordination to appropriate metal ions M^{x+} should provide access to novel oligonuclear aggregates $L_nM[OM\text{-}BH_3]_m$ and supramolecular materials $\{M_n[H_3B\text{-}OM'\text{-}BH_3]_m\}_\infty$ in which classical Werner-type complexes are combined with organometallic moieties. Such compounds would have unique structural properties and may serve as precursors of metal- and boron-containing ceramics.

Our interest in boranes $OM\text{-}BH_2(Do)$ and $(Do)H_2B\text{-}OM'\text{-}BH_2(Do)$ in turn is driven by their potential as precursors to polymeric materials. Chujo et al. have established the hydroboration polymerization of (hetero)aromatic diynes as a powerful tool for the preparation of boron-doped π-conjugated macromolecules with useful optoelectronic properties (cf. **I**, Figure 1).[16−19] Although a broad selection of diynes has already been employed in this reaction, the boron component has remained so far restricted mainly to mesityl- and tripylborane (**I** with R = 2,4,6-trimethylphenyl or 2,4,6-tri-isopropylphenyl). More recently, our groups have reported on the successful use of the difunctional borane reagent 9,10-dihydro-9,10-diboraanthracene in the hydroboration polymerization of 1,4-dialkynylbenzenes.[20] Going one step further, we reasoned that mono- and ditopic organometallic hydroboration reagents could significantly broaden the scope of **I**-type materials if an electronic interaction between the π-conjugated polymer backbone and metal-centered orbitals can be achieved.[21]

Scheme 1. Synthesis of Mono- and Ditopic Ferrocenylhydridoborates **2** and **4**[a]

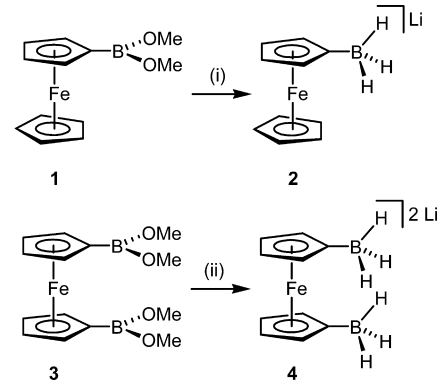

[a] Reagents and conditions: (i) 1 equiv of $Li[AlH_4]$, OEt_2, −78 °C → rt. (ii) 2 equiv of $Li[AlH_4]$, OEt_2, −78 °C → rt.

As an alternative to the hydroboration polymerization approach, we have recently developed a condensation polymerization protocol leading to boron-bridged polyferrocenes **II** (Figure 1) via the reaction of 1,1′-bis(dibromoboryl)ferrocene with triethylsilane.[22] Experimental[22,24] as well as theoretical[22] evidence indicates the initial formation of B(Br)H-containing intermediates, which then undergo polycondensation with liberation of B_2H_6. Polymeric materials may therefore be obtained by either hydroboration or condensation polymerization of compounds $OM\text{-}BH_2(Do)$ and $(Do)H_2B\text{-}OM'\text{-}BH_2(Do)$, and to find suitable conditions for these processes is an intriguing challenge.

This paper describes the synthesis of trihydridoborates $Li[FcBH_3]$ and $Li_2[H_3B\text{-}fc\text{-}BH_3]$, which contain ferrocenyl (Fc) and 1,1′-ferrocenylene (fc), respectively, as organometallic moieties. We will first focus on their solid-state structures to obtain insight into the coordination properties of the anions. In a subsequent step, we will transform these compounds into donor adducts $FcBH_2(Do)$ and $(Do)H_2B\text{-}fc\text{-}BH_2(Do)$ and study the competition between hydroboration and condensation in the presence of suitable olefinic substrates. The last section is then concerned with the application of selected ditopic boranes $(Do)H_2B\text{-}fc\text{-}BH_2(Do)$ to the development of new ferrocene- and boron-containing polymers.

Results and Discussion

The target compounds **2**, **4**, **5**(Do), and **6**$(Do)_2$ are shown in Schemes 1 and 2. Ferrocene was chosen as the organometallic moiety, because it is easy to borylate, diamagnetic, chemically robust, and electrochemically well-behaved.[25,26] As trapping reagents for the ferrocenylboranes **5** and **6**, we tested three Lewis basic donors (Do = NMe_2Et, SMe_2, OEt_2) of significantly

(10) Kot, W. K.; Edelstein, N. M.; Zalkin, A. *Inorg. Chem.* **1987**, *26*, 1339–1341.
(11) Sun, Y.; Spence, R. E. v. H.; Piers, W. E.; Parvez, M.; Yap, G. P. A. *J. Am. Chem. Soc.* **1997**, *119*, 5132–5143.
(12) Spence, R. E. v. H.; Piers, W. E.; Sun, Y.; Parvez, M.; MacGillivray, L. R.; Zaworotko, M. J. *Organometallics* **1998**, *17*, 2459–2469.
(13) Chen, X.; Liu, F.-C.; Plečnik, C. E.; Liu, S.; Du, B.; Meyers, E. A.; Shore, S. G. *Organometallics* **2004**, *23*, 2100–2106.
(14) Ding, E.; Du, B.; Meyers, E. A.; Shore, S. G.; Yousufuddin, M.; Bau, R.; McIntyre, G. J. *Inorg. Chem.* **2005**, *44*, 2459–2464.
(15) Liu, F.-C.; Yang, C.-C.; Chen, S.-C.; Lee, G.-H.; Peng, S.-M. *Dalton Trans.* **2008**, 3599–3604.
(16) Matsumi, N.; Naka, K.; Chujo, Y. *J. Am. Chem. Soc.* **1998**, *120*, 5112–5113.
(17) Matsumi, N.; Miyata, M.; Chujo, Y. *Macromolecules* **1999**, *32*, 4467–4469.
(18) Miyata, M.; Chujo, Y. *Polym. Bull.* **2003**, *51*, 9–16.
(19) Matsumi, N.; Chujo, Y. *Polym. J.* **2008**, *40*, 77–89.
(20) Lorbach, A.; Bolte, M.; Li, H.; Lerner, H.-W.; Holthausen, M. C.; Jäkle, F.; Wagner, M. *Angew. Chem., Int. Ed.* **2009**, *48*, 4584–4588.
(21) Organoboron π-conjugated polymers including Ru-, Pd-, and Pt-alkynyl complexes have been reported: (a) Matsumi, N.; Chujo, Y.; Lavastre, O.; Dixneuf, P. H. *Organometallics* **2001**, *20*, 2425–2427. (b) Matsumoto, F.; Matsumi, N.; Chujo, Y. *Polym. Bull.* **2001**, *46*, 257–262.
(22) Heilmann, J. B.; Scheibitz, M.; Qin, Y.; Sundararaman, A.; Jäkle, F.; Kretz, T.; Bolte, M.; Lerner, H.-W.; Holthausen, M. C.; Wagner, M. *Angew. Chem., Int. Ed.* **2006**, *45*, 920–925.
(23) Scheibitz, M.; Bats, J. W.; Bolte, M.; Lerner, H.-W.; Wagner, M. *Organometallics* **2004**, *23*, 940–942.
(24) Heilmann, J. B.; Qin, Y.; Jäkle, F.; Lerner, H.-W.; Wagner, M. *Inorg. Chim. Acta* **2006**, *359*, 4802–4806.

Scheme 2. Synthesis of Mono- and Ditopic Ferrocenylborane Adducts **5(NMe$_2$Et)**, **5(SMe$_2$)**, **6(NMe$_2$Et)$_2$**, **6(SMe$_2$)$_2$**[a]

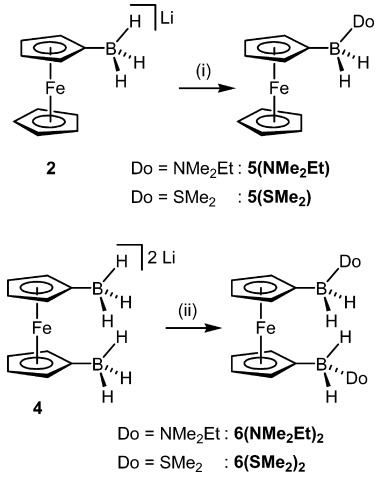

[a] Reagents and conditions: (i) **5(NMe$_2$Et)**, excess Me_3SiCl/excess NMe_2Et, OEt_2, −78 °C → rt; **5(SMe$_2$)**, excess Me_3SiCl, SMe_2, −78 °C → rt. (ii) **6(NMe$_2$Et)$_2$**, excess Me_3SiCl/excess NMe_2Et, OEt_2, −78 °C → rt; **6(SMe$_2$)$_2$**, excess Me_3SiCl, SMe_2, −78 °C → rt.

different donor strengths in order to explore the stability limits of the resulting adducts with respect to the aforementioned condensation reaction.

Ferrocenylhydridoborate Precursors. The ferrocenyl- and 1,1′-ferrocenylenehydridoborates **2** and **4** were prepared from the readily available boronic esters **1**[25] and **3**[25] by treatment with 1 and 2 equiv of $Li[AlH_4]$, respectively (Scheme 1). The structures of **2** and **4** were confirmed by multinuclear NMR spectroscopy and single crystal X-ray diffraction.

The ^{11}B NMR spectra (THF-d_8) of **2** and **4** show quartets at −30.6 ppm ($^1J_{BH}$ = 77.1 Hz) and −33.7 ppm ($^1J_{BH}$ = 79.2 Hz), respectively, which collapse into singlets in the ^1H-decoupled mode. Both chemical shift values are in reasonable agreement with those of other monoorganylhydridoborates (e.g., Li[PhBH$_3$], −26.4 ppm ($^1J_{BH}$ = 76.0 Hz)[27]). In the corresponding ^1H NMR spectra, the hydride ions of the BH_3 substituents give rise to quartets (**2**, $\delta(^1H)$ = 0.86; **4**, $\delta(^1H)$ = 0.75) due to coupling with the ^{11}B nucleus (I = 3/2, natural abundance 80%).[28] In the case of **2**, ^{11}B-coupling is also observed for all carbon atoms of the substituted cyclopentadienyl ring ($\delta(^{13}C)\{^1H\}$ = 67.2 (q, J_{CB} = 2.9 Hz), 75.1 (q, J_{CB} = 3.4 Hz), 92.4 (q, $^1J_{CB}$ = 59.4 Hz)), whereas in the spectrum of **4**, $^{11}B-^{13}C$ coupling is only resolved for the *ipso* carbon resonance ($\delta(^{13}C)\{^1H\}$ = 87.8 (q, $^1J_{CB}$ = 54.3 Hz)).

Compound **2** crystallizes from OEt_2 with 2 equiv of Li^+-coordinated solvent molecules (**2(OEt$_2$)$_2$**), whereas recrystallization of **2(OEt$_2$)$_2$** from pentane at −30 °C leads to the monoether adduct **2(OEt$_2$)**. Crystals of the dilithium salt **4** were also obtained from ethereal solutions. Details of the X-ray crystal structure analyses of **2(OEt$_2$)$_2$**, **2(OEt$_2$)**, and **4(OEt$_2$)$_{2.67}$**, are compiled in Table 1S in Supporting Information.

The crystal lattice of **2(OEt$_2$)$_2$** consists of centrosymmetric dimers that are held together by interactions between two Li^+ ions and two negatively charged trihydridoborate substituents (Figure 2 top). The corresponding distances between the Li^+ ions and the boron atoms are B(1)···Li(1) = 2.511(6) Å and B(1)···Li(1A) = 2.455(6) Å. Using Edelstein's correlation[29] of metal−boron distances as a measure of the denticity of a trihydridoborate group, values of 1.6 ± 0.1 and 1.36 ± 0.06 Å are estimated for the ionic radii of bidentate and tridentate trihydridoborate ligands, respectively. Thus, B···Li distances of about 2.50 and 2.26 Å can be expected for RBH_3-η^2-Li and RBH_3-η^3-Li coordination modes (ionic radii of Li^+ = 0.90 Å (CN 6), 0.73 (CN 4)[30]). This leads to the conclusion that the

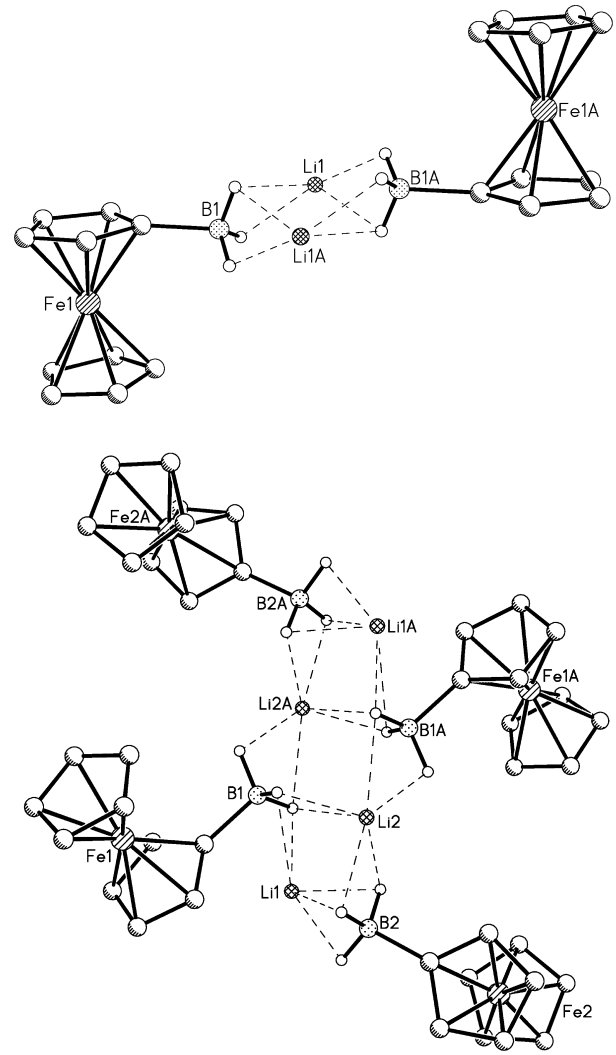

Figure 2. Molecular structures of **2(OEt$_2$)$_2$** (top) and **2(OEt$_2$)** (bottom) in the solid state; hydrogen atoms attached to carbon and Li^+-coordinated OEt_2 molecules have been omitted for clarity. Selected bond lengths (Å), atom···atom distances (Å), and angles (deg): **2(OEt$_2$)$_2$** B(1)−C(1) 1.597(4), B(1)···Li(1) 2.511(6), B(1)···Li(1A) 2.455(6), Li(1)···Li(1A) 3.274(10); B(1)−Li(1)−B(1A) 97.5(2), Li(1)−B(1)−Li(1A) 82.5(2). Symmetry transformation used to generate equivalent atoms: A $-x+1, -y+1, -z+1$. **2(OEt$_2$)** B(1)−C(11) 1.598(4), B(2)−C(31) 1.590(4), B(1)···Li(1) 2.536(5), B(1)···Li(2) 2.579(6), B(1)···Li(2A) 2.553(5), B(2)···Li(1) 2.274(6), B(2)···Li(2) 2.514(6), Li(1)···Li(2) 3.044(7), Li(2)···Li(2A) 3.543(9); B(1)−Li(1)−B(2) 104.9(2), B(1)−Li(2)−B(2) 97.1(2), B(1)−Li(2)−B(1A) 92.7(2),Li(1)−B(1)−Li(2)73.0(2),Li(1)−B(2)−Li(2)78.8(2),Li(2)−B(1)−Li(2A) 87.3(2). Symmetry transformation used to generate equivalent atoms: A $-x+1, -y+1, -z+2$.

(25) Scheibitz, M.; Bolte, M.; Bats, J. W.; Lerner, H.-W.; Nowik, I.; Herber, R. H.; Krapp, A.; Lein, M.; Holthausen, M. C.; Wagner, M. *Chem. Eur. J.* **2005**, *11*, 584–603.
(26) Togni, A.; Hayashi, T. *Ferrocenes*; VCH: Weinheim, 1995.
(27) Singaram, B.; Cole, T. E.; Brown, H. C. *Organometallics* **1984**, *3*, 774–777.
(28) Mason, J. *Multinuclear NMR*; Plenum Press: New York, 1987.
(29) Edelstein, N. *Inorg. Chem.* **1981**, *20*, 297–299.
(30) Shannon, R. D. *Acta Crystallogr.* **1976**, *A32*, 751–767.

trihydridoborate substituents in **2(OEt$_2$)$_2$** act as bidentate ligands and that one H atom at each $[FcBH_3]^-$ moiety is shared between two Li^+ ions. The coordination sphere of each Li^+ ion is completed by two OEt_2 ligands (not shown in Figure 2; cf. Figure 1S in Supporting Information for a complete plot of **2(OEt$_2$)$_2$**).

Recrystallization of **2(OEt$_2$)$_2$** from pentane results in a different crystal structure, **2(OEt$_2$)**, in which each Li^+ ion bears only one OEt_2 ligand (Figure 2 bottom, OEt_2 ligands not shown; cf. Figure 2S in Supporting Information for a complete plot of **2(OEt$_2$)**). In turn, this leads to a higher degree of aggregation so that **2(OEt$_2$)** forms centrosymmetric tetramers in the solid state. The short B(2)···Li(1) distance of 2.274(6) Å indicates a B(2)H$_3$-η^3-Li(1) binding mode. All other B···Li distances fall in the narrow range between 2.514(6) Å−2.579(6) Å, in accord with bidentate coordination of the corresponding trihydridoborate ligands. A closer inspection of the solid-state structure of **2(OEt$_2$)** reveals the following relationship with **2(OEt$_2$)$_2$**: the arrangement of the subunits Fe(1)/B(1), Li(2), Fe(1A)/B(1A), and Li(2A) in **2(OEt$_2$)** closely resembles the dimeric aggregates of **2(OEt$_2$)$_2$**. As a substitute for the missing OEt_2 ligand, $[FcB(2)H_3]^-$ binds to Li(2); the associated $Li(1)^+$ ion adopts a bridging position between B(1) and B(2). We note a further short contact between Li(1) and the *ipso* carbon atom of the Fe(1) ferrocene molecule (Li(1)−C(11) = 2.453(5) Å), which points toward a weak cyclopentadienyl-Li^+ π-interaction.[31,32]

The crystal lattice of **4(OEt$_2$)$_{2.67}$** consists of two different kinds of dimeric entities: dimer(1) contains 5 OEt_2 ligands and possesses C_1 symmetry (Figure 3 top; OEt_2 ligands not shown), whereas the centrosymmetric dimer(2) has 6 OEt_2 ligands coordinated to its Li^+ cations (Figure 3 bottom; OEt_2 ligands not shown; cf. Figure 3S in Supporting Information for a complete plot of **4(OEt$_2$)$_{2.67}$**).

The peripheral alkali metal atoms, Li(1) and Li(2), of dimer(1) are located at bridging positions between the two $[fc(BH_3)_2]^{2-}$ units. Each of these Li^+ ions coordinates to both its hydridoborate ligands in an η^2-mode (range of B···Li distances = 2.48(1) Å−2.61(1) Å) and, in addition, bears two OEt_2 donors. In contrast, the internal $Li(4)^+$ ion is devoid of OEt_2 ligands but establishes close contacts to all four hydridoborate substituents of the dimer.

Judging by the corresponding B···Li distances, both B(3)H$_3$ (2.44(1) Å) and B(4)H$_3$ (2.43(1) Å) fragments act as bidentate ligands, while B(1)H$_3$ (2.67(1) Å) and B(2)H$_3$ (2.68(1) Å) are approaching monodentate binding modes. A highly unusual coordination environment is observed for Li(3): apart from binding one OEt_2 ligand, it interacts with B(1)H$_3$ (2.52(1) Å) and B(2)H$_3$ (2.515(9) Å) and apparently also with the Fe(1) atom (Fe(1)···Li(3) 2.653(9) Å). For geometric reasons, the denticity of B(1)H$_3$ and B(2)H$_3$ cannot exceed the number of 1, even though the short B···Li distances would suggest an η^2-mode. Comparably short Fe···Li distances as in dimer(1) have previously been observed for the lithium salt of a [1.1]diborataferrocenophane, which contains one Li^+ ion at the center of its macrocyclic structure (in this case, the Fe···Li distances amount to 2.706(5) and 2.720(6) Å).[33−35]

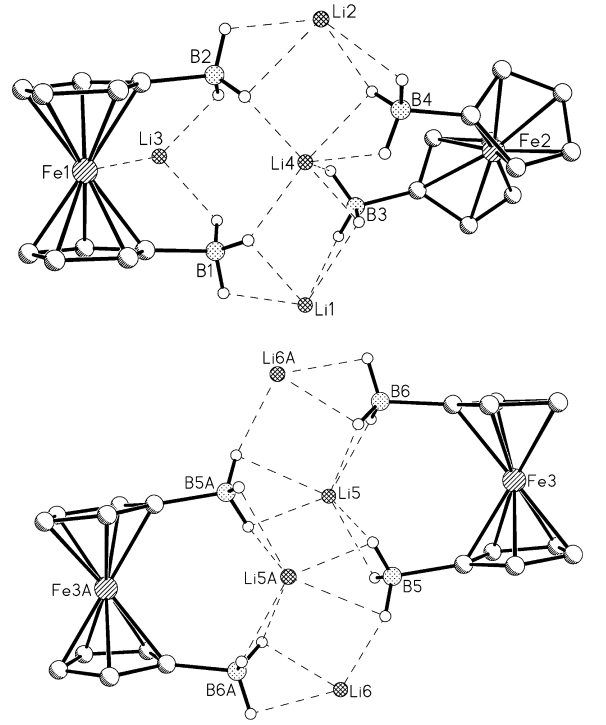

Figure 3. Molecular structure of **4(OEt$_2$)$_{2.67}$** in the solid state; hydrogen atoms attached to carbon and Li^+-coordinated OEt_2 molecules have been omitted for clarity. (Top) dimer(1); (bottom) dimer(2). Selected bond lengths (Å) and atom···atom distances (Å): **Dimer(1)** B(1)−C(11) 1.586(8), B(2)−C(21) 1.584(8), B(3)−C(31) 1.556(8), B(4)−C(41) 1.579(8), B(1)···Li(1) 2.61(1), B(1)···Li(3) 2.52(1), B(1)···Li(4) 2.67(1), B(2)···Li(2) 2.58(1), B(2)···Li(3) 2.515(9), B(2)···Li(4) 2.68(1), B(3)···Li(1) 2.54(1), B(3)···Li(4) 2.44(1), B(4)···Li(2) 2.48(1), B(4)···Li(4) 2.43(1), Fe(1)···Li(3) 2.653(9); **Dimer(2)** B(5)−C(51) 1.579(7), B(6)−C(61) 1.594(7), B(5)···Li(5) 2.516(9), B(5)···Li(5A) 2.59(1), B(5)···Li(6) 2.77(1), B(6)···Li(5) 2.51(1), B(6)···Li(6A) 2.41(1).

Dimer(2) of **4(OEt$_2$)$_{2.67}$** possesses a centrosymmetric structure. Similar to dimer(1), we find two peripheral (Li(6), Li(6A); two OEt_2 ligands) and two internal (Li(5), Li(5A); one OEt_2 ligand) Li^+ ions. In contrast to dimer(1), each Li^+ ion contributes to connecting two $[fc(BH_3)_2]^{2-}$ moieties. Almost all BH_3−Li interactions in dimer(2) are mediated through bidentate bonding modes; the only exception is B(5)H$_3$−Li(6) [B(5A)H$_3$−Li(6A)], which is better described as an η^1-coordination (2.77(1) Å). Moreover, it is worth mentioning that the solid-state structure of dimer(2) is strikingly similar to the structure of 1,1′-

(31) Haghiri Ilkhechi, A.; Scheibitz, M.; Bolte, M.; Lerner, H.-W.; Wagner, M. *Polyhedron* **2004**, *23*, 2597–2604.
(32) Haghiri Ilkhechi, A.; Mercero, J. M.; Silanes, I.; Bolte, M.; Scheibitz, M.; Lerner, H.-W.; Ugalde, J. M.; Wagner, M. *J. Am. Chem. Soc.* **2005**, *127*, 10656–10666.
(33) Scheibitz, M.; Winter, R. F.; Bolte, M.; Lerner, H.-W.; Wagner, M. *Angew. Chem., Int. Ed.* **2003**, *42*, 924–927.
(34) Rodríguez-Otero, J.; Cabaleiro-Lago, E. M.; Peña-Gallego, A.; Montero-Campillo, M. M. *Tetrahedron* **2009**, *65*, 2368–2371.
(35) The interaction of ferrocene with Li^+ in the gas phase has been studied theoretically: Irigoras, A; Mercero, J. M.; Silanes, I.; Ugalde, J. M. *J. Am. Chem. Soc.* **2001**, *123*, 5040–5043. Two minima have been located on the energy surface. In the lower energy structure, the lithium cation is η^5-coordinated on top of one of the cyclopentadienyl rings (cf. Li(1) in **2(OEt$_2$)**). The second minimum structure has the Li^+ ion bonded laterally to the iron atom (Fe···Li = 2.4 Å), which is reminiscent of the situation in dimer(1). Selected related structures of ferrocenyl-Li^+ complexes exhibiting short Fe···Li contacts or ferrocene-Li^+ π-contacts are described in the following references:(a) Walczak, M.; Walczak, K.; Mink, R.; Rausch, M. D.; Stucky, G. *J. Am. Chem. Soc.* **1978**, *100*, 6382–6388. (b) Butler, I. R.; Cullen, W. R.; Reglinski, J.; Rettig, S. J. *J. Organomet. Chem.* **1983**, *249*, 183–194. (c) Sänger, I; Heilmann, J. B.; Bolte, M; Lerner, H.-W.; Wagner, M. *Chem. Commun.* **2006**, 2027–2029. (d) Kaufmann, L.; Vitze, H.; Bolte, M.; Lerner, H.-W.; Wagner, M. *Organometallics* **2007**, *26*, 1771–1776.

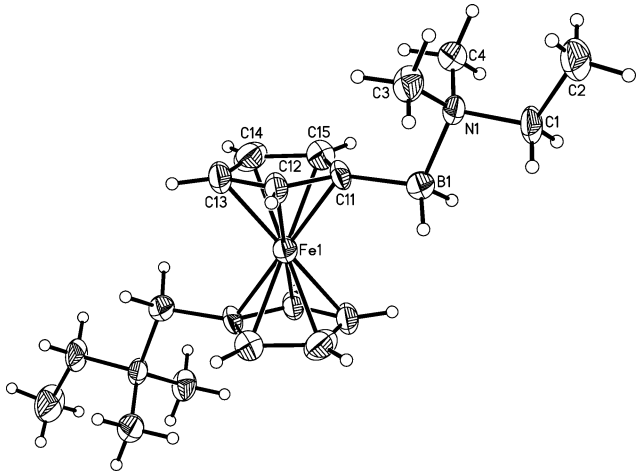

Figure 4. Molecular structure of **6(NMe$_2$Et)$_2$** in the solid state (50% probability ellipsoids). Selected bond lengths (Å), bond angles (deg), and torsion angles (deg): B(1)−N(1) 1.668(12), B(1)−C(11) 1.621(13); N(1)−B(1)−C(11) 111.1(6); N(1)−B(1)−C(11)−C(12) −91.6(10).

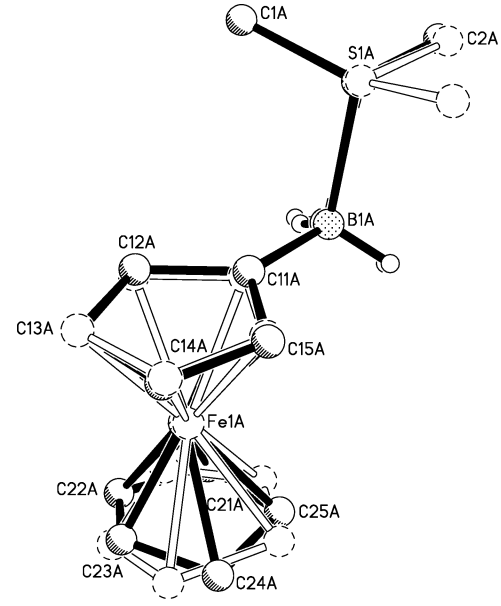

Figure 5. Superposition of the molecular structures of the two crystallographically independent molecules of **5(SMe$_2$)**; hydrogen atoms attached to carbon have been omitted for clarity. Selected bond lengths (Å), bond angles (deg), and torsion angles (deg): **5(SMe$_2$)$_A$** B(1)−S(1) 1.991(11), B(1)−C(11) 1.600(16); S(1)−B(1)−C(11) 107.6(7); S(1)−B(1)−C(11)−C(12) 94.0(12), C(1)−S(1)−B(1)−C(11) 177.7(6), C(2)−S(1)−B(1)−C(11) 73.8(6); **5(SMe$_2$)$_B$**B(1A)−S(1A)1.953(11),B(1A)−C(11A)1.560(18);S(1A)−B(1A)−C(11A) 105.7(6);S(1A)−B(1A)−C(11A)−C(12A)91.7(11),C(1A)−S(1A)−B(1A)−C(11A) −74.8(7), C(2A)−S(1A)−B(1A)−C(11A) −176.8(7).

dilithioferrocene when crystallized from THF (i.e., $Li_4(thf)_6[fc_2]$).[36]

All $[fc(BH_3)_2]^{2-}$ ligands in dimer(1) and dimer(2) adopt eclipsed conformations with both BH_3 substituents pointing into the same direction (range of B−COG−COG′−B′ angles = 4.2−15.9°; COG/COG′ = centroids of the two cyclopentadienyl rings of $Fe(C_5H_4)_2$). The alternative *anti* conformation with B−COG−COG′−B′ angles of around 180°, which would ultimately lead to coordination polymers, is apparently energetically less favorable than the dimeric arrangement with its high charge concentration.

Competition of Condensation and Adduct Formation. We next studied the formation of borane adducts from the hydridoborate species. Abstraction of one hydride ion from **2** by means of Me_3SiCl (which is in turn transformed into Me_3SiH) generates the free ferrocenylborane $FcBH_2$, which spontaneously undergoes condensation to form Fc_2BH (cf. **10**, Scheme 5) and B_2H_6.[23] If, however, hydride elimination is carried out in the presence of NMe_2Et, $FcBH_2$ can be trapped as the B−N adduct $FcBH_2(NMe_2Et)$, **5(NMe$_2$Et)**.[23] Using a similar procedure, the corresponding bis-adduct **6(NMe$_2$Et)$_2$** was obtained from **4(OEt$_2$)$_{2.67}$** and excess Me_3SiCl in OEt_2/NMe_2Et (Scheme 2).

X-ray quality crystals of **6(NMe$_2$Et)$_2$** were grown from a saturated solution in heptane/toluene (1:1) at −30 °C; details of the X-ray crystal structure analysis are provided in Table 2S in Supporting Information. Compound **6(NMe$_2$Et)$_2$** represents one of very few structurally characterized ditopic organoboranes.[20,37−40] The most closely related other example is the diborylmethane-TMEDA adduct $Me_3SiC(H)(BH_2)_2(NMe_2CH_2CH_2NMe_2)$, which forms an unusual seven-membered heterocycle.[40] The molecular structure of **6(NMe$_2$Et)$_2$** is centrosymmetric with the borane substituents pointing into opposite directions (Figure 4). The B−N vectors are almost perpendicular to the planes of the cyclopentadienyl rings (torsion angle N(1)−B(1)−C(11)−C(12) = −91.6(10)). The B(1)−N(1) = 1.668(12) Å bond length is virtually the same as in the monotopic congener **5(NMe$_2$Et)** (1.655(7) Å[23]).

To explore whether the weaker B−S adducts $FcBH_2(SMe_2)$ and $(Me_2S)H_2B$-fc-$BH_2(SMe_2)$ could also be isolated, we treated **2(OEt$_2$)** and **4(OEt$_2$)$_{2.67}$** with excess Me_3SiCl in dry SMe_2 as the solvent. We were indeed able to synthesize and fully characterize the target compounds **5(SMe$_2$)** and **6(SMe$_2$)$_2$** (Scheme 2). The ^{11}B NMR spectrum (SMe_2-d_6) of the ferrocenylborane-SMe_2 adduct **5(SMe$_2$)** is characterized by a triplet at −10.1 ppm ($^1J_{BH}$ = 101.5 Hz). The corresponding signal of **6(SMe$_2$)$_2$** ($\delta(^{11}B) = -7.8$) possesses a width at half height of $h_{1/2}$ = 300 Hz; $^{11}B-^1H$ coupling is not resolved. The ^{11}B NMR resonances for both SMe_2 adducts appear at somewhat higher field compared to the amine adducts (**5(NMe$_2$Et)**, −3.4 ppm (tr, $^1J_{BH}$ = 92.3 Hz);[23] **6(NMe$_2$Et)$_2$**, −2.8 ppm (nr, $h_{1/2}$ = 290 Hz); C_6D_6). All ^1H and $^{13}C\{^1H\}$NMR data of **5(SMe$_2$)**, **6(SMe$_2$)$_2$**, and **6(NMe$_2$Et)$_2$** are fully in accord with the proposed structures and therefore do not merit further discussion.

5(SMe$_2$) crystallizes from SMe_2 with two crystallographically independent molecules in the asymmetric unit (**5(SMe$_2$)$_A$**, **5(SMe$_2$)$_B$**; see Table 2S in Supporting Information for details of the X-ray crystal structure). The major difference between **5(SMe$_2$)$_A$** and **5(SMe$_2$)$_B$** lies in the orientation of the two methyl groups relative to the ferrocenyl fragment (cf. Figure 5 for a superposition of **5(SMe$_2$)$_A$** and **5(SMe$_2$)$_B$**; an ORTEP plot of **5(SMe$_2$)$_A$** is shown in Figure 4S in Supporting Information).

To a first approximation, **5(SMe$_2$)$_A$** and **5(SMe$_2$)$_B$** are mirror images of each other. Upon detailed examination, however, it becomes evident that the conformations of the two ferrocenyl substituents are different, namely, eclipsed in **5(SMe$_2$)$_A$**, but staggered in **5(SMe$_2$)$_B$**. The B−S bond lengths of **5(SMe$_2$)** amount to 1.991(11) and 1.953(11) Å. The only other structur-

(36) Sánchez Perucha, A.; Heilmann-Brohl, J.; Bolte, M.; Lerner, H.-W.; Wagner, M. *Organometallics* **2008**, *27*, 6170–6177.
(37) Yalpani, M.; Boese, R.; Köster, R. *Chem. Ber.* **1987**, *120*, 607–610.
(38) Baker, R. T.; Ovenall, D. W.; Harlow, R. L.; Westcott, S. A.; Taylor, N. J.; Marder, T. B. *Organometallics* **1990**, *9*, 3028–3030.
(39) Paetzold, P.; Englert, U.; Finger, R.; Schmitz, T.; Tapper, A.; Ziembinski, R. *Z. Anorg. Allg. Chem.* **2004**, *630*, 508–518.
(40) Zheng, C.; Hosmane, N. S. *Acta Crystallogr.* **1999**, *C55*, 2107–2109.

Scheme 3. Preparation of Cyclohexyldi(ferrocenyl)borane **7** and Tricyclohexylborane **8** by Reaction of the Ferrocenylhydridoborate **2** with Me_3SiCl in the Presence of Cyclohexene[a]

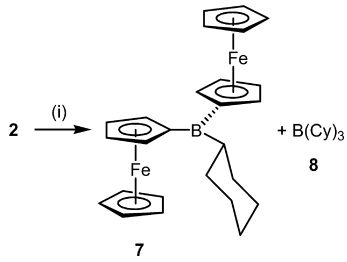

[a] Reagents and conditions: (i) excess Me_3SiCl/excess C_6H_{10}, OEt_2, −78 °C → rt.

Scheme 4. Synthesis of Boron-Bridged Polyferrocene **9**[a]

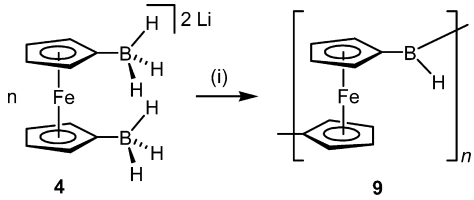

[a] Reagents and conditions: (i) excess Me_3SiCl, Me_2S, −78 °C → rt.

ally characterized SMe_2 adduct of a monoorganylborane is the dimeric species $(MeSCH_2BH_2)_2$.[41] This six-membered heterocycle possesses B−S bond lengths of 1.951(2) Å, which compare nicely with the values determined for **5(SMe$_2$)**.

When instead of SMe_2, OEt_2 was used as reaction solvent, we were not able to isolate or even detect the respective adducts $FcBH_2(OEt_2)$ and $(Et_2O)H_2B$-fc-$BH_2(OEt_2)$ but rather observed spontaneous condensation to Fc_2BH (**10**) and [-fcB(H)-]$_n$ (**9**; vide infra).

Competition of Condensation and Hydroboration. The successful isolation of compounds **5(Do)** and **6(Do)$_2$** clearly shows that $FcBH_2$ and H_2B-fc-BH_2 more readily undergo B-NMe_2Et and B-SMe_2 (but not B-OEt_2) adduct formation than condensation to Fc_2BH (**10**) and [-fcB(H)-]$_n$ (**9**). This result immediately raises the question whether $FcBH_2$ could also be trapped by hydroboration before substituent scrambling occurs. To answer this question, we treated a solution of **2(OEt$_2$)** and 8 equiv of cyclohexene in OEt_2 with excess Me_3SiCl (Scheme 3). After workup, the hydroboration product (**7**) of Fc_2BH was isolated in almost 65% yield. The structure of **7** was confirmed by multinuclear NMR ($\delta(^{11}B) = 66.2$) and single crystal X-ray crystallography (Figure 5S in Supporting Information). We also obtained crystals of $B(Cy)_3$ (**8**; Cy = cyclohexyl, Figure 6S in Supporting Information), which apparently forms by reaction of the second condensation product, B_2H_6, with cyclohexene. On the other hand, there was no indication for the presence of $FcB(Cy)_2$, and we therefore conclude that the rate of condensation of $FcBH_2$ to Fc_2BH is much higher than that of hydroboration of an internal *cis*-olefin by $FcBH_2$.[42]

Condensation Polymerization. 6(NMe$_2$Et)$_2$ was first examined as a potential precursor for the formation of a ferrocenylborane polymer, [-fcB(H)-]$_n$ (**9**; Scheme 4), via condensation polymerization. For this process to occur efficiently, the amine donor needs to reversibly dissociate from the borane moieties. NMR studies of **6(NMe$_2$Et)$_2$** in C_6D_6 solution did not show any indication of polymerization of the ditopic borane at room temperature (rt). We then studied the possible thermal polymerization in the solid state by thermogravimetric analysis. A multistep profile was observed (cf. Figure 7S in Supporting Information); the first step with an onset at ca. 125 °C leads to ca. 7% weight loss, followed by a distinct second step with ca. 30% further weight loss occurring over the temperature range from 130 to 300 °C. These two processes likely correspond to loss of the amine ligands and possibly formation of a polymeric species similar to **9** with concomitant liberation of borane. Above 300 °C, slow further degradation is observed with the residual weight at 800 °C amounting to ca. 25% of the initial sample weight. The latter observation would be consistent with formation of a ceramic material from a polymeric species.[43] However, although the results indicate that a polymeric species may be formed upon thermolysis of **6(NMe$_2$Et)$_2$**, we reasoned that use of a weaker donor should promote the polymerization process and ultimately allow for rt polymerization to occur.

Indeed, we found that both **5(SMe$_2$)** and **6(SMe$_2$)$_2$** slowly undergo condensation even in SMe_2 solutions. On a preparative scale, we treated the precursor **4** in SMe_2 with Me_3SiCl, thereby generating the diadduct **6(SMe$_2$)$_2$** as described above, which was expected to polymerize slowly and in a very controlled manner. After a reaction time of 7 d (the reaction rate can be increased by diluting the SMe_2 with CH_2Cl_2), the mixture was worked up, the crude product was reprecipitated from CH_2Cl_2 into hexane, and dried under reduced pressure. The polymeric borane **9** was obtained as a pale red, air-sensitive powdery solid. However, based on its ^1H NMR data, the product was contaminated with small quantities of $BH_3(SMe_2)$, which were surprisingly difficult to remove completely. However, we found that **9** could be easily prepared by treatment of **4** with Me_3SiCl in OEt_2 and simple evaporation of the mixture to dryness after completion of the condensation. All further studies (vide infra) were carried out on samples synthesized via this reaction protocol.

Hydroboration of Diferrocenylborane and Poly(ferrocenylborane). To develop a clean, high-yielding reaction protocol for transformation of the primary polymer **9** into more stable and better soluble macromolecules, we first screened several carbonyl compounds, alkenes, and alkynes in the hydroboration reaction with the dinuclear model compound Fc_2BH (**10**; Scheme 5). Phenylacetylene and *tert*-butylacetylene turned out to be the reagents of choice, because they gave the corresponding di(ferrocenyl)vinylboranes **11^{Ph}** and **11^{tBu}** in virtually quantitative yield (NMR spectroscopic control; cf. Figure 8S in Supporting Information for a ^1H NMR spectrum recorded on the crude reaction mixture of **10** and *t*BuCCH). Typical of triorganylboranes,[44] the vinylboranes **11^{Ph}** and **11^{tBu}** generate low-field signals at 56.7 ppm (**11^{Ph}**) and 57.2 ppm (**11^{tBu}**) in their $^{11}B\{^1H\}$ NMR spectra. The chemical composition of the molecules (i.e., ferrocenyl/vinyl = 2:1) is confirmed by the proton integral ratios of the organyl substituents. $^3J_{HH}$ coupling constants of about 18 Hz within the vinyl moieties of **11^{Ph}** and **11^{tBu}** point toward *trans* arrangements of the vinyl protons, which is in line with the expected *cis* addition of boranes to alkynes.

(41) Nöth, H.; Sedlak, D. *Chem. Ber.* **1983**, *116*, 1479–1486.
(42) Cyclohexene was used in this experiment to circumvent potential regioselectivity issues. It should be noted, however, that the reactivity of a terminal alkene can be higher than that of cyclohexene.
(43) Manners, I. *Science* **2001**, *294*, 1664–1666.
(44) Nöth, H.; Wrackmeyer, B. Nuclear magnetic resonance spectroscopy of boron compounds. In *NMR Basic Principles and Progress*; Diehl, P., Fluck, E., Kosfeld, R., Eds.; Springer: Berlin, Heidelberg, New York, 1978.

Scheme 5. Hydroboration of PhCCH or *t*BuCCH with Ferrocenylborane **10** and Polymer **9**[a]

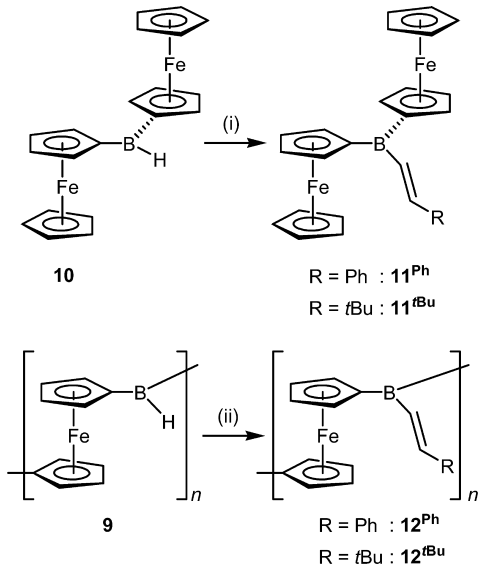

[a] Reagents and conditions: (i) **11**^{Ph}, 1 equiv of PhCCH, toluene, rt; **11**^{tBu}, excess *t*BuCCH, hexane, 35 °C, ultrasonication. (ii) **12**^{Ph}, excess PhCCH, toluene, 50 °C; **12**^{tBu}, excess *t*BuCCH, toluene, ultrasonication at rt and 50 °C.

NMR spectroscopic investigations into the stability of **11**^{Ph} and **11**^{tBu} toward oxygen and moisture were carried out by exposing C_6D_6 solutions of the compounds to air. Under these conditions, only 5% of **11**^{Ph} was left after 4 h, whereas the relative amount of **11**^{tBu} with respect to all decomposition products was about 90% after 4 h and still 45% after 25 h, suggesting that a reasonably stable polymeric derivative of **9** should be accessible by hydroboration with *tert*-butylacetylene.

We performed hydroborations with polymer **9**, which was generated in situ from **4**, using both PhCCH and *t*BuCCH. Suspensions of **9** were prepared in toluene, the respective alkyne was added at rt, and the mixtures were heated to 50 °C (application of ultrasound increases the reaction rate). The products were obtained as reddish solids upon evaporation of the solvents, washed with hexanes and reprecipitated from CH_2Cl_2 (**12**^{Ph}) or toluene (**12**^{tBu}) into hexane. Successful hydroboration was confirmed by IR and NMR spectroscopy.

The individual NMR assignments were established by comparison of the data for the polymers with those of the model systems **11**^{Ph} and **11**^{tBu}, for which C,H-COSY was used to unequivocally assign all resonances. Polymers **12**^{Ph} and **12**^{tBu} show broad signals attributable to the 1,1′-ferrocenylene moieties (ca. 4.2−4.7 ppm) as well as the phenyl (**12**^{Ph}, 6.9−7.6 ppm) and *tert*-butyl groups (**12**^{tBu}, 0.9−1.1 ppm). Most importantly, a new set of vinyl resonances was observed at 6.2, 6.6 ppm for **12**^{tBu}, in the same region as for the model compound **11**^{tBu} (6.32, 6.70 ppm). For polymer **12**^{Ph}, the vinyl protons overlap with the aromatic protons in the region from 6.9−7.6 ppm, as is the case for dimer **11**^{Ph} (7.24, 7.53 ppm). The generation of olefinic groups at the polymer side chains was further confirmed by the presence of intense C=C stretching bands at 1611 cm^{-1} (**12**^{Ph}) and 1623 cm^{-1} (**12**^{tBu}), which lie in the typical range of alkenylboranes[45] (cf. **11**^{Ph}, 1608 cm^{-1}; **11**^{tBu}, 1604 cm^{-1}).

Polymer Characterization. Our attempts at determining the molecular weight of the polymers by gel permeation chromatography (GPC) analysis in THF did not provide any tangible results, presumably due to the sensitivity of **12**^{Ph} and **12**^{tBu} toward air and moisture. The polymers were then subjected to dynamic light scattering in toluene solution under a nitrogen atmosphere. However, the scattering intensity was too weak to determine a reliable average hydrodynamic radius (R_h), which suggests that the polymer chain lengths are relatively short and the number average molecular weight (M_n) is ≤5000.[46] This result is consistent with prior studies on the related polymer [-fcB(Mes)-]$_n$, which was shown by GPC with in-line multiangle laser light scattering detection (GPC-MALLS) to have a M_n of 5160.[22]

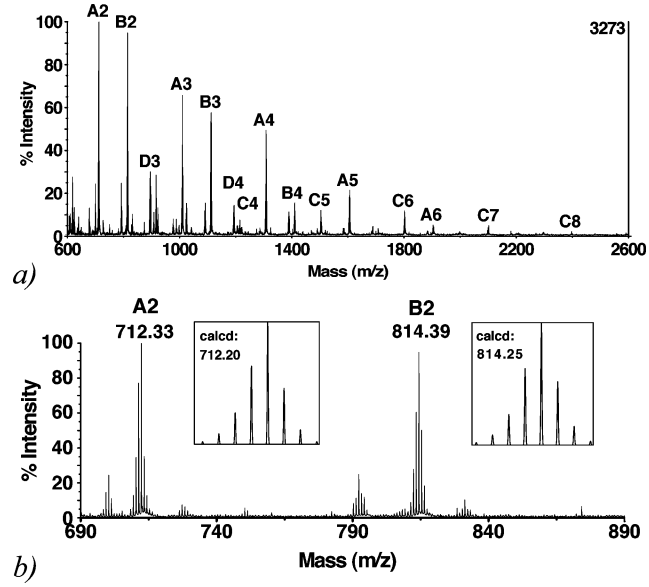

Figure 6. (a) MALDI-TOF mass spectrum of polymer **12**^{Ph} acquired in (+) ion reflector mode. The different series are indicated as A, B, C, and D; the numbers of the individual peaks correspond to the number of repeating units. (b) Expansion of the mass range from 690 to 890 Da and comparison of the peak patterns with those calculated assuming a 10000:1 resolving power.

To confirm the polymer structure and to examine the polymer end groups, we studied both polymers **12**^{Ph} and **12**^{tBu} by high resolution MALDI-TOF mass spectrometry in (+) ion reflector mode. The spectrum of **12**^{Ph} shows a complex pattern with multiple series of peaks (Figure 6).

Importantly, for each of the independent series in **12**^{Ph} the mass difference between peaks correlates well with that expected for the repeating unit of [fcB(CH=CHPh)] ($C_{18}H_{15}B_1Fe_1$, 298 Da). The same is true for the spectrum of **12**^{tBu} (cf. Figure 9S in Supporting Information), in which the peak separation corresponds to the expected repeating unit of [fcB(CH=CH*t*Bu)] ($C_{16}H_{19}B_1Fe_1$, 278 Da). In the following, the different peak series are discussed in more detail for the Ph derivative **12**^{Ph}; very similar results were also obtained for **12**^{tBu}.

Most of the major peak series can be assigned with confidence by comparison of the individual peak patterns with those calculated assuming a 10 000:1 resolving power. We find that the series labeled as A2−A6 in Figure 6 with peak maxima of 712.33, 1010.44, 1307.55, 1606.66, and 1903.78 fits reasonably well to polymers of the formula {(PhCH=CH)HB-[fcB(CH=CHPh)]$_n$-H}$^+$ (n = 2−6), thus suggesting the presence of [BH(CH=CHPh)]

(45) Zweifel, G.; Clark, G. M.; Leung, T.; Whitney, C. C. *J. Organomet. Chem.* **1976**, *117*, 303–312.

(46) Berenbaum, A.; Braunschweig, H.; Dirk, R.; Englert, U.; Green, J. C.; Jäkle, F.; Lough, A. J.; Manners, I. *J. Am. Chem. Soc.* **2000**, *122*, 5765–5774.

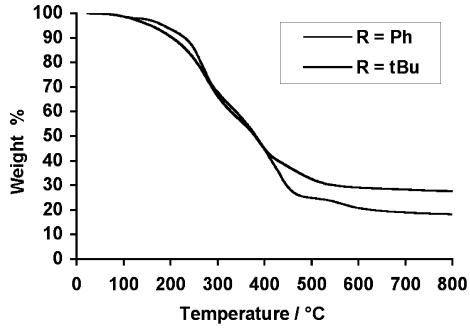

Figure 7. Thermogravimetric analysis plots of $\mathbf{12^{Ph}}$ and $\mathbf{12^{tBu}}$.

moieties at both chain ends. Series B2−B4 with peak maxima at 814.39, 1112.50, and 1410.62 closely matches the peak positions expected for polymers in which one of the chain ends underwent a second hydroboration reaction, i.e., $\{(PhCH{=}CH)_2B\text{-}[fcB(CH{=}CHPh)]_n\text{-}H\}^+$ (n = 2−4). The third series that is labeled as C4−C8 with peak maxima at 1206.49, 1503.60, 1801.71, 2099.82, and 2397.89 is likely also related to series A (n = 4−8), but one of the boron centers along the polymer chain has not undergone hydroboration, i.e. an additional BH functionality remains. Finally, the peaks labeled as D3 (895.36) and D4 (1194.46) are tentatively attributed to polymers in which there is a monoborylated ferrocenyl moiety ($C_{10}H_9Fe$) at one chain end, while the other chain end features a [BH(CH=CHPh)] group, i.e., $\{H\text{-}[fcB(CH{=}CHPh)]_n\text{-}H\}^+$.

The thermal stability of polymers $\mathbf{12^{Ph}}$ and $\mathbf{12^{tBu}}$ was examined by thermogravimetric analysis (Figure 7). The onset of degradation of polymer [-fcB(CH=CHPh)-]$_n$ ($\mathbf{12^{Ph}}$) was determined by TGA under nitrogen to be ca. 185 °C (5% weight loss). A multistep degradation process was observed over the temperature range from 160 to 550 °C and the residual weight at 800 °C was 18%. A similar profile was also observed for [-fcB(CH=CH*t*Bu)-]$_n$ ($\mathbf{12^{tBu}}$) with an onset of degradation of 160 °C (5% weight loss) and a residual weight of 28% at 800 °C. The thermal stability of both polymers is somewhat lower than that of the mesityl-substituted derivative [-fcB(Mes)-]$_n$, which showed a single-step weight loss of 72%, with an inflection point at 403 °C, and gave a brown ceramic material in 28% yield.[22] The different behavior may be related to the higher stability of mesitylboranes in comparison to vinylborane derivatives.[47]

Electronic Structure of Polymers and Model Systems. One of the key questions with regard to the electronic properties of polymers derived from **9** is whether a conformation is possible that allows for efficient π-conjugation of the ferrocenes via the empty *p*-orbital of the boron bridge. In this context, the model compounds $\mathbf{11^{Ph}}$ and $\mathbf{11^{tBu}}$ were further investigated by X-ray crystallography. Details of the X-ray crystal structure analyses of $\mathbf{11^{Ph}}$ and $\mathbf{11^{tBu}}$ are included into Table 3S in Supporting Information, and the structure plots are displayed in Figure 8. Both molecules contain a trigonal-planar boron center and the two ferrocenyl substituents adopt an *anti* conformation with respect to the C(1)B(1)C(11)C(31) plane. Most importantly, an inspection of the dihedral angles between the C_5H_4 rings and the C(1)B(1)C(11)C(31) plane reveals values of 12.3°/21.1° for $\mathbf{11^{Ph}}$ and of about 17° for $\mathbf{11^{tBu}}$, which is an ideal precondition for substantial π-electron delocalization. Interestingly, the related dihedral angle spanned by the plane of the olefinic double bond

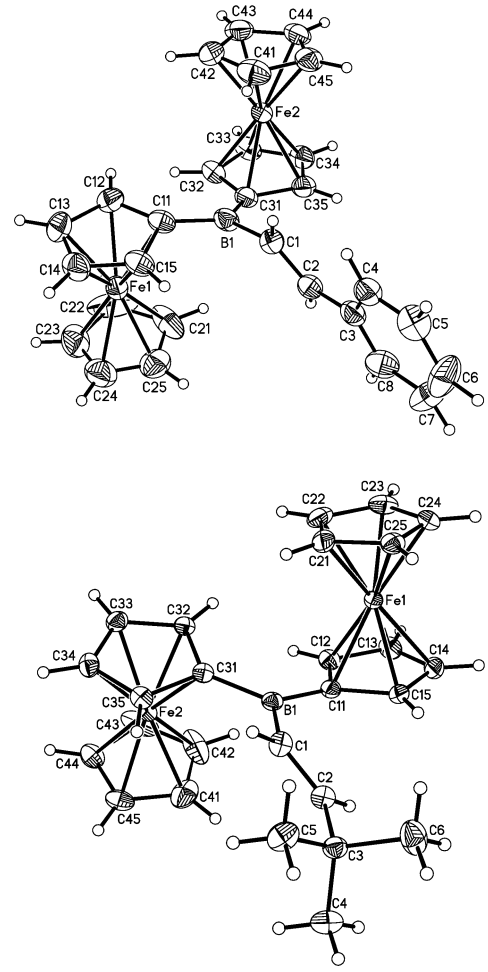

Figure 8. Molecular structures of $\mathbf{11^{Ph}}$ (top) and $\mathbf{11^{tBu}}$ (bottom) in the solid state (30% and 50% probability ellipsoids, respectively). Selected bond lengths (Å), bond angles (deg), torsion angles (deg), and dihedral angles (deg) for $\mathbf{11^{Ph}}$: B(1)−C(1) 1.575(9), B(1)−C(11) 1.551(7), B(1)−C(31) 1.552(6),C(1)−C(2) 1.340(17);C(1)−B(1)−C(11) 111.5(4),C(1)−B(1)−C(31) 122.4(4),C(11)−B(1)−C(31) 126.0(4),B(1)−C(1)−C(2) 124.3(9),C(1)−C(2)−C(3) 124.2(9); C(2)−C(1)−B(1)−C(11) −123.1(6), C(2)−C(1)−B(1)−C(31) 60.8(7); B(1)C(1)C(2)//C(1)B(1)C(11)C(31) 58.7, C(11) to C(15) ring// C(1)B(1)C(11)C(31) 21.1, C(31) to C(35) ring//C(1)B(1)C(11)C(31) 12.3. For $\mathbf{11^{tBu}}$: B(1)−C(1) 1.576(2), B(1)−C(11) 1.562(2), B(1)−C(31) 1.562(2), C(1)−C(2) 1.340(2); C(1)−B(1)−C(11) 120.8(1), C(1)−B(1)−C(31) 116.4(1), C(11)−B(1)−C(31) 122.9(1), B(1)−C(1)−C(2) 126.0(2), C(1)−C(2)−C(3) 129.2(2); C(2)−C(1)−B(1)−C(11) −33.8(2), C(2)−C(1)−B(1)-C(31) 148.2(2); B(1)C(1)C(2)//C(1)B(1)C(11)C(31) 32.7, C(11) to C(15) ring// C(1)B(1)C(11)C(31) 17.2, C(31) to C(35) ring//C(1)B(1)C(11)C(31) 17.1.

(i.e., B(1)C(1)C(2)) and C(1)B(1)C(11)C(31) is only 32.7° for $\mathbf{11^{tBu}}$ (58.7° for $\mathbf{11^{Ph}}$), most likely in order to minimize unfavorable steric interactions.

Consistent with these findings, the longest wavelength absorption maxima in the UV−vis spectra in toluene show distinct bathochromic shifts for the polymers ($\mathbf{12^{Ph}}$, λ_{max} = 495 nm; $\mathbf{12^{tBu}}$, λ_{max} = 482 nm) in comparison to the dimeric model systems ($\mathbf{11^{Ph}}$, λ_{max} = 484 nm; $\mathbf{11^{tBu}}$, λ_{max} = 472 nm), accompanied by distinct tailing to longer wavelengths (cf. Figure 10S in Supporting Information).

Conclusion

This paper reports on the first examples of mono- and ditopic trihydridoborates and -boranes with organometallic substituents, i.e., Li[FcBH$_3$] (**2**; Fc = ferrocenyl), Li$_2$[H$_3$B-fc-BH$_3$] (**4**; fc =

(47) Entwistle, C. D.; Marder, T. B. *Angew. Chem., Int. Ed.* **2002**, *41*, 2927–2931.

1,1′-ferrocenylene), $FcBH_2$ (**5**), and H_2B-fc-BH_2 (**6**). The hydridoborate salts **2** and **4** not only serve as precursors for **5** and **6** but also are potentially useful ligands for the generation of inorganic/organometallic hybrid compounds. Especially the ditopic species $[H_3B\text{-fc-}BH_3]^{2-}$ holds great promise in this respect, because its anionic groups are connected by a flexible ferrocenylene hinge that allows an *anti* conformation of the donor sites, which should lead to coordination polymers, as well as a *syn* conformation, which should lead to metalla-macrocycles. A crystal structure analysis of the ether solvate of the lithium salt **4** revealed several structural peculiarities: (i) macrocyclic dimers are formed, in which four Li^+ ions and two iron atoms are brought into close proximity; (ii) some of the Li^+ ions adopt bridging positions between the two $[Cp\text{-}BH_3]^-$ ligands of the same Fe(II) center, which is reminiscent of an *ansa*-ferrocene motif; and (iii) the solid-state structure of **4** is strikingly similar to the structure of the THF-solvate of 1,1′-dilithioferrocene.[36]

The ferrocenylboranes $FcBH_2$ (**5**) and H_2B-fc-BH_2 (**6**) can be isolated and fully characterized only as donor adducts $FcBH_2$(Do) (**5(Do)**) and (Do)H_2B-fc-BH_2(Do) (**6(Do)$_2$**; Do = NMe_2Et, SMe_2). In the absence of suitable Lewis bases, **5** and **6** tend to undergo a condensation reaction leading to Fc_2BH (**10**) and the polymer [-fcB(H)-]$_n$ (**9**), respectively, with concomitant liberation of B_2H_6. This condensation is much faster than the hydroboration of internal olefins as demonstrated in a competition experiment, in which $FcBH_2$ (**5**) was generated in the presence of excess cyclohexene. In this experiment, Fc_2BCy was formed as the major ferrocene-containing product (condensation pathway, 2 $FcBH_2$ + excess cyclohexene → Fc_2BCy + BCy_3, as opposed to hydroboration pathway, $FcBH_2$ + excess cyclohexene → $FcBCy_2$).

The novel polymer [-fcB(H)-]$_n$ (**9**), which is obtained upon spontaneous condensation of **6**, is interesting in its own right, as it represents a rare example of a polymeric material with multiple reactive borane groups.[48] We exploited the ability of these borane functionalities to undergo hydroboration reactions for the preparation of new boron-bridged polyferrocenes. Indeed, treatment of **9** with the alkynes PhCCH and *t*BuCCH leads to smooth conversion to vinylborane polymers [-fcB(CH═CHR)]$_n$ (**12^{Ph}**, R = Ph; **12^{tBu}**, R = *t*Bu). The polymer structures were confirmed by NMR and IR spectroscopy, as well as MALDI-TOF mass spectrometry. Interestingly, extended delocalization via the boron empty *p*-orbitals is suggested by distinctly red-shifted absorption maxima in the UV−vis spectra of the polymers compared to the dinuclear model compounds Fc_2B(CH═CHR) (**11^{Ph}**, R = Ph; **11^{tBu}**, R = *t*Bu). Favorable electronic delocalization is also consistent with the structural features deduced from the X-ray structure of the dimeric species **11^{Ph}** and **11^{tBu}**, in which the C_5H_4 rings are almost coplanar to the planes defined by the boron atom and the attached carbon substituents.

With this work we have established a viable pathway to electronically interesting boron-containing metallopolymers, which complements the ring-opening polymerization of boron-bridged ferrocenophanes[46,49] and the condensation polymerization of fc(BBr_2)$_2$ with $HSiEt_3$.[22] The primary polymer obtained in our new approach, i.e., [-fcB(H)-]$_n$, can be functionalized by a broad variety of derivatization reactions. Work is in progress to apply this new method also to the development of other organic and organometallic polymeric materials.

(48) Doshi, A.; Jäkle, F. *Main Group Chem.* **2006**, *5*, 309–318.
(49) Braunschweig, H.; Dirk, R.; Müller, M.; Nguyen, P.; Resendes, R.; Gates, D. P.; Manners, I. *Angew. Chem., Int. Ed. Engl.* **1997**, *36*, 2338–2340.

Experimental Methods

General Remarks. All reactions were carried out under a nitrogen atmosphere using Schlenk tube techniques. Reaction solvents were either freshly distilled under argon from Na/Pb alloy (alkanes) and Na/benzophenone (toluene, C_6D_6, OEt_2, THF-d_8) or dried over molecular sieves (4 Å; CH_3CN, $CDCl_3$, CH_2Cl_2, SMe_2, SMe_2-d_6) prior to use. NMR: Bruker AM 250, Avance 300, Avance 400, and Varian 500. Chemical shifts are referenced to residual solvent signals (^1H, $^{13}C\{^1H\}$) or external $BF_3\cdot OEt_2$ ($^{11}B\{^1H\}$). Abbreviations: s = singlet, d = doublet, tr = triplet, vtr = virtual triplet, q = quartet, m = multiplet, br = broad, no = signal not observed, nr = signal not resolved, Ph = phenyl. $FcB(OMe)_2$ (**1**),[25] fc$(B(OMe)_2)_2$ (**3**),[25] and Fc_2BH (**10**)[23] were synthesized following literature procedures.

Synthesis of Li[$FcBH_3$] (2). A solution of Li[AlH_4] in OEt_2 (1 M; 10.6 mL, 10.6 mmol) was added dropwise with stirring at −78 °C to a solution of **1** (2.72 g, 10.55 mmol) in OEt_2 (20 mL). After 30 min, the mixture was allowed to warm to rt and stirred for 1 h. The insolubles were collected on a frit (G4) and washed with OEt_2 (3 × 10 mL). The volume of the filtrate was slowly reduced under vacuum, whereupon large yellow crystals of Li$(OEt_2)_2$[$FcBH_3$] (**2(OEt$_2$)$_2$**) formed, which were suitable for X-ray crystallography. Crystals of the monoether adduct Li(OEt_2)[$FcBH_3$] (**2(OEt$_2$)**) were grown from a saturated solution of **2(OEt$_2$)$_2$** in pentane at −30 °C. Yield of **2(OEt$_2$)$_2$**: 2.83 g (76%). ^1H NMR (400.1 MHz, THF-d_8, 300 K): δ 0.86 (q, $^1J_{BH}$ = 77.1 Hz, 3H; BH_3), 3.75 (nr, 4H; C_5H_4), 3.81 (s, 5H; C_5H_5). $^{13}C\{^1H\}$ NMR (62.9 MHz, THF-d_8, 300 K): δ 67.2 (q, J_{CB} = 2.9 Hz; C_5H_4), 68.3 (C_5H_5), 75.1 (q, J_{CB} = 3.4 Hz; C_5H_4), 92.4 (q, $^1J_{CB}$ = 59.4 Hz; CB). ^{11}B NMR (128.4 MHz, THF-d_8, 300 K): δ −30.6 (q, $^1J_{BH}$ = 77.1 Hz). Elemental analysis calcd (%) for $C_{18}H_{32}BFeLiO_2$ (354.04): C 61.07, H 9.11. Found: C 60.51; H 8.98.

Synthesis of Li$_2$[fc(BH_3)$_2$] (4). A solution of Li[AlH_4] in OEt_2 (1 M; 11.0 mL, 11.0 mmol) was added dropwise with stirring at −78 °C to a solution of **3** (1.81 g, 5.49 mmol) in OEt_2 (20 mL). After 30 min, the mixture was allowed to warm to rt and stirred for 1 h. The insolubles were collected on a frit (G4) and washed with OEt_2 (4 × 15 mL). The volume of the filtrate was slowly reduced under vacuum, whereupon large yellow crystals of Li$_2(OEt_2)_{2.67}$[fc$(BH_3)_2$] (**4(OEt$_2$)$_{2.67}$**) formed, which were suitable for X-ray crystallography. Yield of **4(OEt$_2$)$_{2.67}$**: 1.70 g (73%). ^1H NMR (400.1 MHz, THF-d_8, 300 K): δ 0.75 (q, $^1J_{BH}$ = 79.2 Hz, 6H; BH_3), 3.51, 3.75 (2 × nr, 2 × 4H; C_5H_4). $^{13}C\{^1H\}$ NMR (62.9 MHz, THF-d_8, 303 K): δ 68.0, 74.4 (C_5H_4), 87.8 (q, $^1J_{CB}$ = 54.3 Hz; CB). ^{11}B NMR (128.4 MHz, THF-d_8, 300 K): δ −33.7 (q, $^1J_{BH}$ = 79.2 Hz). Elemental analysis calcd (%) for $C_{41.33}H_{81.33}B_4Fe_2Li_4O_{5.33}$ (846.43): C 58.65, H 9.68. Found: C 58.18; H 9.50.

Synthesis of $FcBH_2$(SMe_2) (5(SMe_2)). Me_3SiCl (0.50 mL, 0.43 g, 3.95 mmol) in SMe_2 (5 mL) was added dropwise with stirring at −78 °C to a solution of **2(OEt$_2$)** (0.190 g, 0.68 mmol) in SMe_2 (5 mL). After 30 min, the mixture was allowed to warm to 0 °C, then stirred for 1 h, warmed to rt, and filtered over a frit (G4). The volume of the filtrate was reduced to 2 mL, and the remaining solution was stored at −30 °C for 3 d, whereupon **5(SMe_2)** crystallized in the form of long orange needles, which were suitable for X-ray crystallography. Yield: 0.148 g (84%). ^1H NMR (250.1 MHz, SMe_2-d_6, 297 K): δ 2.05 (s, 6H; CH_3), 2.60 (br, 2H; BH_2), 3.93 (nr, 2H; C_5H_4), 3.99 (s, 5H; C_5H_5), 4.07 (nr, 2H; C_5H_4). $^{13}C\{^1H\}$ NMR (62.9 MHz, SMe_2-d_6, 297 K): δ 18.0 (CH_3), 68.2 (C_5H_5), 69.7, 75.4 (C_5H_4), no (CB). ^{11}B NMR (128.4 MHz, SMe_2-d_6, 297 K): δ −10.1 (tr, $^1J_{BH}$ = 101.5 Hz).

Synthesis of fc(BH_2(SMe_2))$_2$ (6(SMe_2)$_2$). Me_3SiCl (0.50 mL, 0.43 g, 3.95 mmol) in SMe_2 (5 mL) was added dropwise with stirring at −78 °C to a solution of **4(OEt$_2$)$_{2.67}$** (0.265 g, 0.63 mmol) in SMe_2 (10 mL). After 30 min, the mixture was allowed to warm

to 0 °C, then stirred for 1 h, warmed to rt, and filtered over a frit (G4). The volume of the filtrate was reduced to 3 mL, and the remaining solution was stored at −30 °C for 3 d, whereupon **6(SMe$_2$)$_2$** precipitated as yellow microcrystalline solid. Yield: 0.191 g (91%). ^{1}H NMR (250.1 MHz, SMe$_2$-d_6, 297 K): δ 2.05 (s, 12H; CH_3), 2.54 (br, 4H; BH_2), 3.80, 3.96 (2 × nr, 2 × 4H; C_5H_4). ^{13}C{^{1}H} NMR (62.9 MHz, SMe$_2$-d_6, 297 K): δ 18.0 (CH_3), 70.2, 75.4 (C_5H_4), no (CB). ^{11}B NMR (128.4 MHz, SMe$_2$-d_6, 297 K): δ −7.8 (nr, $h_{1/2}$ = 300 Hz).

Synthesis of fc(BH$_2$(NMe$_2$Et))$_2$ (6(NMe$_2$Et)$_2$). Me$_3$SiCl (1.5 mL, 1.28 g, 11.74 mmol) in OEt$_2$ (5 mL) was added dropwise with stirring at −78 °C to a solution of **4(OEt$_2$)$_{2.67}$** (0.412 g, 0.97 mmol) and NMe$_2$Et (1.00 mL, 0.68 g, 9.30 mmol) in OEt$_2$ (20 mL). After 30 min, the mixture was allowed to warm to 0 °C, then stirred for 1 h, warmed to rt, and filtered over a frit (G4). The volume of the filtrate was reduced to 5 mL, and the remaining solution was stored at −30 °C for 24 h, whereupon **6(NMe$_2$Et)$_2$** precipitated as yellow microcrystalline solid. Yield: 0.318 g (92%). X-ray quality crystals were grown from a saturated solution of **6(NMe$_2$Et)$_2$** in heptane/toluene (1:1) at −30 °C. ^{1}H NMR (250.1 MHz, C_6D_6, 300 K): δ 0.58 (tr, $^3J_{HH}$ = 7.3 Hz, 6H; CH_2CH_3), 1.86 (s, 12H; NCH_3), 2.31 (q, $^3J_{HH}$ = 7.3 Hz, 4H; CH_2CH_3), 2.88 (very br, 4H; BH_2), 4.41 (m, 8H; C_5H_4). ^{13}C{^{1}H} NMR (62.9 MHz, C_6D_6, 300 K): δ 8.2 (CH_2CH_3), 47.2 (NCH_3), 55.7 (CH_2CH_3), 70.5, 76.8 (C_5H_4), no (CB). ^{11}B NMR (128.4 MHz, C_6D_6, 303 K): δ −2.8 (nr, $h_{1/2}$ = 290 Hz). Elemental analysis calcd (%) for $C_{18}H_{34}B_2FeN_2$ (355.94): C 60.74, H 9.63. Found: C 60.55; H 9.61.

Synthesis of Fc$_2$BCy (7) and BCy$_3$ (8). Me$_3$SiCl (0.50 mL, 0.43 g, 3.95 mmol) in OEt$_2$ (5 mL) was added dropwise with stirring at −78 °C to a solution of **2(OEt$_2$)** (0.130 g, 0.46 mmol) and cyclohexene (0.39 mL, 0.32 g, 3.90 mmol) in OEt$_2$ (5 mL). The mixture was allowed to warm to rt, stirred for 1 h, and filtered over a frit (G4). The insolubles were washed with OEt$_2$ (2 × 5 mL), and the combined organic phases evaporated to dryness under vacuum. The solid residue was dissolved in a minimum amount of warm heptane, and the solution was stored at −30 °C, whereupon dark orange colored crystals of **7** precipitated during a time span of 12 h. Yield of **7**: 0.068 g (64%). Colorless needles of **8** were obtained by storing the mother liquid at −30 °C for several days. Analytical data of **7**: ^{1}H NMR (250.1 MHz, C_6D_6, 300 K): δ 1.22−2.11 (m, 11H; C_6H_{11}), 4.01 (s, 10H; C_5H_5), 4.43, 4.64 (2 × nr, 2 × 4H; C_5H_4). ^{13}C{^{1}H} NMR (62.9 MHz, C_6D_6, 300 K): δ 27.8, 29.0, 31.1 (C_6H_{11}), 69.0 (C_5H_5), 73.5, 76.8 (C_5H_4), no (CB). ^{11}B NMR (128.4 MHz, C_6D_6, 300 K): δ 66.2 ($h_{1/2}$ = 390 Hz). Elemental analysis calcd (%) for $C_{26}H_{29}BFe_2$ (464.00): C 67.30, H 6.30. Found: C 67.00; H 6.18. Analytical data of **8**: ^{1}H NMR (250.1 MHz, C_6D_6, 300 K): δ 1.00−2.07 (m, 33H; C_6H_{11}). ^{13}C{^{1}H} NMR (62.9 MHz, C_6D_6, 300 K): δ 26.9, 27.4, 27.7 (C_6H_{11}), no (CB). ^{11}B NMR (128.4 MHz, C_6D_6, 300 K): δ 81.8 ($h_{1/2}$ = 530 Hz).

Synthesis of Fc$_2$B(CH=CHPh) (11^{Ph}). Neat PhCCH (0.11 mL, 0.10 g, 1.00 mmol) was added via syringe to a stirred solution of **10** (0.377 g, 0.99 mmol) in toluene (40 mL). After the mixture had been stirred for 24 h at rt, all volatiles were removed at 50 °C under vacuum. Recrystallization of the crude material from H$_3$CCN (25 mL) gave dark red X-ray quality crystals of **11^{Ph}**. Yield: 0.198 g (41%). ^{1}H NMR (250.1 MHz, $CDCl_3$, 300 K): δ 4.10 (s, 10H; C_5H_5), 4.66 (nr, 8H; C_5H_4), 7.24 (d, $^3J_{HH}$ = 18.1 Hz, 1H; C_2H_2), 7.36 (m, 1H; Ph-H$_p$), 7.42 (vtr, 2H; Ph-H$_m$), 7.53 (d, $^3J_{HH}$ = 18.1 Hz, 1H; C_2H_2), 7.65 (d, $^3J_{HH}$ = 7.3 Hz, 2H; Ph-H$_o$). ^{1}H NMR (300.0 MHz, C_6D_6, 300 K): δ 4.00 (s, 10H; C_5H_5), 4.49, 4.69 (2 × vtr, 2 × 4H; C_5H_4), 7.13 (m, 1H; Ph-H$_p$), 7.22 (vtr, 2H; Ph-H$_m$), 7.43 (d, $^3J_{HH}$ = 18.2 Hz, 1H; C_2H_2), 7.59 (d, $^3J_{HH}$ = 7.4 Hz, 2H; Ph-H$_o$), 7.73 (d, $^3J_{HH}$ = 18.2 Hz, 1H; C_2H_2). ^{13}C{^{1}H} NMR (75.5 MHz, $CDCl_3$, 300 K): δ 69.1 (C_5H_5), 73.7, 76.3 (C_5H_4), 126.9 (Ph−C$_o$), 128.2 (Ph−C$_p$), 128.7 (Ph−C$_m$), 134.0, 144.8 (C_2H_2), no (Ph−C$_i$, CB). ^{11}B NMR (96.3 MHz, $CDCl_3$, 300 K): δ 56.7 ($h_{1/2}$ = 500 Hz). IR (cm^{-1}): 1608 (C=C-Ph). UV−vis (nm): λ_{max}(0.1 mM, toluene) = 380, 484. Elemental analysis calcd (%) for $C_{28}H_{25}BFe_2$ (483.99): C 69.48, H 5.21. Found: C 69.08; H 5.28.

Synthesis of Fc$_2$B(CH=CH*t*Bu) (11^{tBu}). Neat *t*BuCCH (0.25 mL, 0.17 g, 2.05 mmol) was added via syringe to a stirred suspension of **10** (0.310 g, 0.81 mmol) in hexane (40 mL). After the mixture had been heated to 35 °C in an ultrasonic bath for 3 h, all volatiles were removed under vacuum. Recrystallization of the crude material from hot H$_3$CCN (7.5 mL) gave red X-ray quality crystals of **11^{tBu}**. Yield: 0.366 g (97%). ^{1}H NMR (250.1 MHz, $CDCl_3$, 300 K): δ 1.17 (s, 9H; CH_3), 4.06 (s, 10H; C_5H_5), 4.59 (nr, 8H; C_5H_4), 6.32, 6.70 (2 × d, $^3J_{HH}$ = 18.1 Hz, 2 × 1H; C_2H_2). ^{1}H NMR (300.0 MHz, C_6D_6, 300 K): δ 1.16 (s, 9H; CH_3), 4.00 (s, 10H; C_5H_5), 4.47, 4.66 (2 × vtr, 2 × 4H; C_5H_4), 6.54, 6.84 (2 × d, $^3J_{HH}$ = 18.1 Hz, 2 × 1H; C_2H_2). ^{13}C{^{1}H} NMR (75.5 MHz, C_6D_6, 300 K): δ 29.6 (CH_3), 35.1 ($C(CH_3)_3$), 69.4 (C_5H_5), 73.9, 76.7 (C_5H_4), 128.8, 159.7 (C_2H_2), no (CB). ^{11}B NMR (96.3 MHz, C_6D_6, 300 K): δ 57.2 ($h_{1/2}$ = 500 Hz). IR (cm^{-1}): 1604 (C=C-*t*Bu). UV−vis (nm): λ_{max}(0.1 mM, toluene) = 359, 472. Elemental analysis calcd (%) for $C_{26}H_{29}BFe_2$ (464.00): C 67.30, H 6.30. Found: C 67.16; H 6.35.

Synthesis of [-fcB(H)-]$_n$ (9). Me$_3$SiCl (0.50 mL, 0.43 g, 3.95 mmol) in SMe$_2$ (5 mL) was added dropwise with stirring at −78 °C to a solution of **4(OEt$_2$)$_{2.67}$** (0.239 g, 0.56 mmol) in SMe$_2$ (10 mL). After 30 min, the mixture was allowed to warm to 0 °C, stirred for 1 h at this temperature, warmed to rt, and then filtered over a frit (G4). The filtrate was stirred for 7 d at rt, whereupon it adopted a deep red color. The volatiles were driven off under reduced pressure, CH_2Cl_2 (5 mL) was added to the solid residue, and small quantities of insoluble material were removed by filtration. The filtrate was added dropwise to hexane (10 mL), whereupon **9** precipitated as pale red solid that was collected on a frit and washed with hexane (3 × 5 mL). The isolated product was dried under vacuum overnight. Yield: 0.070 g (64%). ^{1}H NMR (250.1 MHz, $CDCl_3$, 300 K): δ 4.0−4.2 (~ 0.7H; chain termini, C_5H_5), 4.2−4.5, 4.5−4.7 (2 × very br, 2 × 4H; C_5H_4) 5.7 (very br, 1H; BH). ^{13}C{^{1}H} NMR (100.6 MHz, $CDCl_3$, 300 K): δ 67.0−70.5 (very br; chain termini, C_5H_5), 71.4−79.1 (very br; C_5H_4), no (CB). ^{11}B NMR (128.4 MHz, $CDCl_3$, 300 K): δ 51.6 ($h_{1/2}$ = 1200 Hz). IR (cm^{-1}): 2360, 2341 (B−H).

Synthesis of [-fcB(CH=CHPh)-]$_n$ (12^{tPh}). Neat Me$_3$SiCl (1.30 mL, 1.11 g, 10.22 mmol) was added via syringe at −78 °C to a stirred solution of **4(OEt$_2$)$_{2.67}$** (0.515 g, 1.21 mmol) in OEt$_2$ (30 mL). The mixture was first stirred for 1 h and then allowed to warm to rt. Volatiles were removed under vacuum and the residue was treated with a solution of PhCCH (0.60 mL, 0.56 g, 5.48 mmol) in toluene (30 mL). The resulting mixture was heated to 50 °C for 8 h. After filtration, the filtrate was evaporated to dryness under vacuo and the solid residue was washed with hexane (3 × 10 mL) to remove unreacted PhCCH. The reddish solid obtained was dissolved in a minimum amount of CH_2Cl_2 and precipitated into hexane. Yield: 0.24 g (66%). ^{1}H NMR (500 MHz, $CDCl_3$): δ 4.2−4.7 (br, 8H; C_5H_4), 6.9−7.6 (br, 7H; C_6H_5, C_2H_2). IR (cm^{-1}): 1611 (C=C-Ph). UV−vis (nm): λ_{max}(0.1 mM, toluene) = 378, 495 (shoulder).

Synthesis of [-fcB(CH=CH*t*Bu)-]$_n$ (12^{tBu}). Neat Me$_3$SiCl (0.60 mL, 0.51 g, 4.70 mmol) was added via syringe at −78 °C to a stirred solution of **4(OEt$_2$)$_{2.67}$** (0.224 g, 0.53 mmol) in OEt$_2$ (15 mL). The mixture was first stirred for 1 h and then allowed to warm to rt. Volatiles were removed under vacuum and the residue was treated with a solution of *t*BuCCH (0.35 mL, 0.23 g, 2.85 mmol) in toluene (15 mL). The resulting mixture was stirred at rt for 2 h, it was then ultrasonicated for 3 h at rt, and for 4 h at 50 °C. After filtration, the filtrate was evaporated to dryness under vacuum. The residue was dissolved in a minimum amount of toluene and precipitated into hexane. Yield: 0.062 (42%). ^{1}H NMR (500 MHz, $CDCl_3$): δ 0.9−1.1 (br, 9H; *t*Bu), 4.2−4.7 (br, 8H; C_5H_4), 6.2, 6.6 (br, 2H; C_2H_2). IR (cm^{-1}): 1623 (C=C-*t*Bu). UV−vis (nm): λ_{max}(0.1 mM, toluene) = 362, 482 (shoulder).

Crystal Structure Analyses. Crystals of **2(OEt$_2$)$_2$**, **2(OEt$_2$)**, **4(OEt$_2$)$_{2.67}$**, **5(SMe$_2$)**, **6(NMe$_2$Et)$_2$**, **11^{Ph}**, and **11^{tBu}** were measured on a STOE IPDS-II diffractometer with graphite-monochromated

Mo Kα radiation. An empirical absorption correction with program PLATON[50] was performed for all structures. The structures were solved by direct methods using the program SHELXS[51] and refined with full-matrix least-squares on F^2 using the program SHELXL97.[52] Hydrogen atoms were placed on ideal positions and refined with fixed isotropic displacement parameters using a riding model. One ether molecule in **4(OEt$_2$)$_{2.67}$** is disordered over two sites with occupation factors 0.52(1) and 0.48(1). **5(SMe$_2$)** was a racemic twin with a ratio of the twin components of 0.50(8):0.50(8). In **11^{Ph}**, the atoms C(1) and C(2) constituting the olefinic bond are disordered over two positions with occupancy factors of 0.74(2) and 0.26(2). CCDC reference numbers: 740781 (**2(OEt$_2$)$_2$**), 740782 (**2(OEt$_2$)**), 740783 (**4(OEt$_2$)$_{2.67}$**), 740784 (**5(SMe$_2$)**), 740785 (**6(NMe$_2$Et)$_2$**), 740789 (**11^{Ph}**), 740786 (**11^{tBu}**).

Thermal Analyses of Polymers. Thermogravimetric analysis (TGA) was performed under N_2 atmosphere using a Perkin-Elmer Pyris 1 system with ca. 4−5 mg of polymer at a heating rate of 20 °C/min from 30 to 800 °C.

Mass Spectrometry of Polymers. MALDI-TOF measurements were performed on an Applied Biosystems 4700 (**12^{Ph}**) or 4800 (**12^{tBu}**) Proteomics Analyzer in (+) ion reflectron mode with delayed extraction. Benzo[a]pyrene was used as the matrix (20 mg/mL in toluene). Samples were prepared in toluene (10 mg/mL), mixed with the matrix in a 1:10 ratio, and then spotted on the wells of a sample plate inside a glovebox. Peptides were used for calibration (Des-Arg-Bradykinin (904.4681), Angiotensin I (1296.6853), Glu-Fibrinopeptide B (1570.6774), ACTH (clip 1−17) (2093.0867), ACTH (clip 18−39) (2465.1989), ACTH (clip 7−38) (3657.9294) with α-hydroxy-4-cyanocinnamic acid as the matrix).

(50) Spek, A. L. *J. Appl. Crystallogr.* **2003**, *36*, 7–13.
(51) Sheldrick, G. M. *Acta Crystallogr.* **1990**, *A46*, 467–473.
(52) Sheldrick, G. M. *SHELXL-97. A Program for the Refinement of Crystal Structures*; Universität Göttingen: Göttingen, 1997.

Acknowledgment. M.W. is grateful to the Deutsche Forschungsgemeinschaft (DFG) and the Fonds der Chemischen Industrie (FCI) for financial support. F.J. thanks the Alexander von Humboldt Foundation for a Friedrich Wilhelm Bessel Research Award. M.S. has been financially supported by a Ph.D. grant of the Fonds der Chemischen Industrie (FCI) and the Bundesministerium für Bildung und Forschung (BMBF).

Supporting Information Available: Crystallographic data for all structurally characterized compounds in tabular form; ORTEP-plots of **2(OEt$_2$)$_2$**, **2(OEt$_2$)**, **4(OEt$_2$)$_{2.67}$**, and **5(SMe$_2$)$_A$**; ORTEP plots and a compilation of selected bond lengths and angles of **7** and **8**; cif files of all structures determined by X-ray crystallography; thermogravimetric analysis plot of **6(NMe$_2$Et)$_2$**; ^{1}H NMR spectrum of the crude product of the hydroboration of *t*BuCCH with Fc_2BH (**10**); MALDI-TOF mass spectrum of polymer **12^{tBu}**; comparison of the UV−vis spectra of **11^{Ph}/12^{Ph}** and **11^{tBu}/12^{tBu}**. This material is available free of charge via the Internet at http://pubs.acs.org.

JA906575S